

# Performance Modeling of Next-Generation Wireless Networks

Antonios Michaloliakos, Ryan Rogalin, Yonglong Zhang, Konstantinos Psounis, *Senior Member, IEEE* and Giuseppe Caire, *Fellow, IEEE*

**Abstract**—The industry is satisfying the increasing demand for wireless bandwidth by densely deploying a large number of access points which are centrally managed, e.g. enterprise WiFi networks deployed in university campuses, companies, airports etc. This “small cell” architecture is gaining traction in the cellular world as well, as witnessed by the direction in which 4G+ and 5G standardization is moving. Prior academic work in analyzing such large-scale wireless networks either uses oversimplified models for the physical layer, or ignores other important, real-world aspects of the problem, like MAC layer considerations, topology characteristics, and protocol overhead. On the other hand, the industry is using for deployment purposes on-site surveys and simulation tools which do not scale, cannot efficiently optimize the design of such a network, and do not explain why one design choice is better than another.

In this paper we introduce a simple yet accurate analytical model which combines the realism and practicality of industrial simulation tools with the ability to scale, analyze the effect of various design parameters, and optimize the performance of real-world deployments. The model takes into account all central system parameters, including channelization, power allocation, user scheduling, load balancing, MAC, advanced PHY techniques (single and multi user MIMO as well as cooperative transmission from multiple access points), topological characteristics and protocol overhead. The accuracy of the model is verified via extensive simulations and the model is used to study a wide range of real world scenarios, providing design guidelines on the effect of various design parameters on performance.

## I. INTRODUCTION

Modern wireless devices such as tablets and smartphones are pushing the demand for higher and higher wireless data rates while causing significant stress to existing wireless networks. While successive generations of wireless standards achieve continuous improvement, it is the general understanding of both academic research and the industry that a significant increase in wireless traffic demand can be met only by a dramatically denser spectrum reuse, i.e., by deploying more base stations/access points per square kilometer, coupled with advanced physical (PHY) layer techniques to reduce inter-cell interference.

Enterprise WiFi networks have been deployed following this paradigm for years. As a matter of fact, the density of access points (APs) has increased to a point where inter-cell interference is canceling any additional gains from even denser deployments. At the same time, advanced physical layer techniques have been incorporated into the standards, most notably single-user MIMO in 802.11n and multi-user MIMO in 802.11ac. Cellular networks, unable to satisfy the

bandwidth demand of data plans, resort to WiFi offloading, i.e. they deploy WiFi networks to offload the cellular network. Future cellular network architectures will most likely follow a similar pattern, that is, they will consist of many small cells densely deployed and use advanced physical layer techniques, e.g. massive MIMO.

It is evident that a wireless network consisting of a large number of small, overlapping cells cannot be left to operate in a completely decentralized manner. The industry has responded to the need to efficiently managing such networks with tools which are mostly based on on-site measurements, simulations, and over-simplistic analytical models. Based on the available public information about such tools in the enterprise WiFi market [1], [2], these tools perform three main operations: (i) user load balancing among APs, (ii) interference management between APs by channel allocation and power control, and (iii) optimization of the Clear Channel Assessment (CCA) CSMA threshold to allow for concurrent transmissions which can tolerate interference from nearby APs. While such network management tools have increased the performance of enterprise WiFi networks, they do not scale well, cannot be used to efficiently optimize the system, and do not incorporate the effects of advanced physical layer techniques.

In this paper, we introduce an accurate and practical analytical model which takes into consideration all the important parameters affecting the performance of present and future wireless networks, and can be efficiently used in real-world setups. Specifically, we model and investigate the performance impact of physical layer features such as channelization, power allocation, topological characteristics (e.g. user density and AP distribution in various buildings/structures) and physical layer techniques like single-user (SU), multi-user (MU), and distributed MU-MIMO [3], [4] (where a number of remote APs coordinate and transmit concurrently and jointly to multiple users). Additionally, we model the performance impact of MAC and higher layer features such as user-AP association, MAC parametrization and adaptive coding/modulation.

Our main contributions are the following. We introduce and validate through simulations the first (to the best of our knowledge) analytical model which can be applied in real-world scenarios while taking into account all the important design parameters in the PHY, MAC and higher layers. Second, we apply the model to next generation wireless networking technologies such as MU-MIMO and distributed MU-MIMO for which there is currently no clear understanding of large scale network performance. Third, we apply the model to a variety of real world scenarios, including conference halls,

office buildings, open spaces, large stadiums, etc., and study a number of important phenomena including the impact of different channelization options (e.g. using the whole bandwidth as a complete, continuous channel vs. chopping it down to multiple channels to mitigate interference), the effect of the CSMA CCA threshold in user throughput under the different wireless technologies, the performance of a well-deployed, close to ideal CSMA based network under different technologies, the degradation of performance from using realistic quantized rates based on the Modulation and Coding schemes (MCS), etc. (see Section VI for a detailed discussion).

The outline of the paper is as follows. In the next section we discuss related work. In Section III we discuss basic PHY characteristics. Section IV motivates and describes a unified analytic treatment of wireless network deployments consisting of an analytical model for various current and next generation PHY layer schemes as well as for CSMA MAC. The validation and limitations of our model are studied via extensive simulations for tractable scenarios of interest in Section V. Finally Section VI applies the analytic model in various deployment scenarios of interest like conference halls, open and closed office floor plans and stadiums.

## II. RELATED WORK

The wide adoption of wireless networks both as infrastructure and especially as end-user connectivity has attracted the interest of many research communities, namely those of communication/information theory and networking.

There are two main trends the communication literature follows in analyzing wireless network deployments. The first makes use of techniques based on random matrix theory to extract performance measures (such as achievable rates, SINRs etc.) combined with combinatorial and convex optimization methods to solve problems that appear in multi-cell wireless networks. Such problems include but are not limited to: finding the optimal achievable rates under power control, massive MIMO system asymptotics, base station cooperation towards a distributed MU-MIMO solution and more as can be found in prior work of ours [5]–[7] and others [8]–[13]. The second approach is based on stochastic geometry results and focus on the spatial configuration modeling of random placement of APs and users according some stochastic point process (see for example [14] and references therein for such works). The developed techniques have been extensively applied in heterogeneous cellular networks on problems such as: load balancing [15], user-AP association [16] and K-tier base station modeling [17]. Most of these works do not consider MIMO and advanced interference management schemes at the PHY layer since they introduce statistical dependence between the nodes, and this would break the independence on which most of these results are based. Also, a common theme of the aforementioned information theoretic literature is that they almost invariably neglect the MAC scheduling algorithms that all wireless networks make use of. We propose a simple analytic approach that incorporates PHY layer advances as the ones mentioned above in a single PHY/MAC layer model.

On the other hand, the networking community looked at this problem from a different angle: early work of Bianchi [18],

[19] on 802.11 MAC layer proposed an analytical model to analyze CSMA/CA overhead and performance. Meanwhile in [20] the authors investigated the performance of exponential backoff mechanism in terms of throughput and delay. In [21]–[24] similar Markov Chain models of CSMA/CA have been developed and employed to develop algorithms optimizing various performance metrics. Finally, in our own previous works [25], [26], a full analytic model for computing the achievable rate region of CSMA in multi hop wireless networks has been presented. These works are mostly based on pure upper layer modeling and do not take the advances of physical layer into account, which is the main contribution of this particular paper. A few recent papers have taken limited steps towards such a combination but lack the analytic simplicity our model has, and limit their results to standard simulation based approaches [27] or neglect MAC considerations all together [28].

Lastly, there are a number of tools that the industry currently uses for wireless network deployment guidance. For example, Fluke Networks has developed a product [29] which creates a model for the wireless environment so that an administrator may simulate and predict the performance. These tools mostly resort to real time on-site surveys which do not scale and do not incorporate state-of-the-art advances in the PHY layer.

## III. NEXT-GENERATION WI-FI PRIMER

**OFDM primer.** Orthogonal Frequency Division Multiplexing (OFDM) [30] is the preferred PHY layer modulation technique of modern cellular and WLAN networks. OFDM consists of taking blocks of  $N$  coded modulation “frequency domain” symbols and transforming them into a block of  $N$  “time domain chips” via an Inverse Discrete Fourier Transform (IDFT). Each block of  $N$  time-domain chips is expanded by repeating the last  $L$  chips at the beginning of the block. This precoding technique, known as Cyclic Prefixing (CP), is able to turn the linear convolution of the transmitted signal with the channel impulse response into a block-by-block cyclic convolution, provided that the length of the multipath channel (in chips) is not larger than  $L$ . At the receiver, after block timing and carrier frequency synchronization, the CP is removed and a DFT is applied to the resulting blocks of  $N$  chips in order to recover the  $N$  frequency domain symbols. As a result, the time-domain multipath channel is transformed into a set of parallel frequency-flat channels (referred to as subcarriers) in which each frequency-domain symbol experiences only a complex multiplicative “fading” channel coefficient, corresponding approximately to the channel transfer function evaluated at each subcarrier center frequency (see [31] for a recent accurate and general model of OFDM including also non-ideal transmit/receive effects).

**Topology and pathloss model.** We define a region based on some topology and a fine, regular grid of quantized coordinates, with some geometry of walls and blocking objects (e.g., buildings in an outdoor campus scenario, or office walls in an indoor building scenario). Access points (APs) and user terminals (UTs) are located at the nodes of the grid, and are placed in scenario-dependent locations.

**Small-scale fading.** It is well-known that typical wireless channels in WLAN environments are slowly-varying in time.

For a sequence of successive time slots, each one corresponding to a data packet, the channel coefficients are strongly correlated such that estimates obtained at a given point in time are accurate for a fairly large number of time slots [30].

Motivated by this, in the following we assume that the frequency-domain channel coefficients are random but constant over many data slots, and drop the time index when referring to a time slot for the sake of notation simplicity. We shall use index  $\nu$  to indicate the OFDM subcarrier index. Hence, the channel between an AP  $i$  equipped with  $M$  antennas and a user terminal (UT)  $k$  equipped with a single antenna at any given generic time slot and OFDM subcarrier  $\nu$  is given by

$$y_k[\nu] = \sqrt{g_{ik}} \mathbf{x}_i[\nu]^H \mathbf{h}_{ik}[\nu] + z_k[\nu], \quad (1)$$

where  $\mathbf{h}_{ik}[\nu]$  is an  $M \times 1$  vector with Gaussian i.i.d. elements  $\sim \mathcal{CN}(0, 1)$ ,<sup>1</sup> representing the channel coefficients between the antenna array of AP  $i$  and the antenna of UT  $k$ ,  $\mathbf{x}_i[\nu]$  is a  $M \times 1$  vector containing the (frequency-domain) coded modulation symbols sent by AP  $i$  in the downlink, on subcarrier  $\nu$ , and  $z_k[\nu]$  collects noise plus the interference caused by other APs transmitting on the same time slot and frequency channel at the receiver of UT  $k$ . The channel gain  $g_{ik}$  is a function of the distance between AP  $i$  and UT  $k$  and of other “large-scale” effects, such as blocking objects, walls and trees. This “large-scale” channel gain is frequency-flat, i.e., it does not depend on the subcarrier index  $\nu$ , and it is modeled using the widely accepted WINNER-II model [32].

**MIMO primer.** Point-to-Point MIMO [33], [34] consists of the techniques of extracting higher capacities from a given wireless bandwidth by adding antennas to the transmitter and receiver. MIMO is ideally suited to work together with OFDM. We describe the effective channel between a transmitter with  $N_t$  antennas and a receiver with  $N_r$  antennas via a set of  $N_t \times N_r$  channel matrices  $\mathbf{H}_{ik}[\nu]$  for all the subcarriers forming the given system channel. One of the advantages of having multiple transmit/receive antennas is the ability to increase the effective SNR, known as a power gain. For example, using maximal ratio combining [30] in a  $1 \times N_r$  channel, the effective received signal SNR is multiplied by  $\|\mathbf{h}_{ik}[\nu]\|^2$ . In the downlink, if AP  $i$  has  $N_t > 1$  antennas and UT  $k$  has only a single antenna, knowledge of the  $N_t \times 1$  downlink channel vector  $\mathbf{h}_{ik}[\nu]$  can be used to perform conjugate beamforming (aka maximal ratio beamforming) in order to achieve the same SNR gain  $\|\mathbf{h}_{ik}[\nu]\|^2$  [30]. In addition, a variety of techniques globally known as *spatial precoding* [30] enable multiplexing in the spatial domain, such that the capacity at high SNR is increased by a *multiplicative factor* up to  $\min(N_t, N_r)$ , referred to as “multiplexing gain” or “degrees of freedom (DoFs) gain.”

With Point-to-Point MIMO, a multiplexing gain larger than 1 is achievable only if multiple antennas are used on both the transmitter and the receiver side (i.e.,  $\min\{N_t, N_r\} > 1$ ). Particularly for the downlink this may represent a significant

<sup>1</sup> $h \sim \mathcal{CN}(0, 1)$  indicates a complex circularly symmetric Gaussian random variable with mean 0 and variance  $\mathbb{E}[|h|^2] = 1$ . This type of small-scale fading is usually referred to as Rayleigh fading [30].

limitation since, as mentioned before,  $N_r$  may be small (1 or at most 2). In this case, a set of techniques known as multiuser MIMO (MU-MIMO) [35] can be used to attain higher multiplexing gain up to  $\min\{M, KN_r\}$ , for a system where an AP with  $M$  antennas serves  $K$  UTs with  $N_r$  antennas each. Since the UTs do not cooperate, most MU-MIMO schemes require channel state information at the transmitter (CSIT) in order to precode the data streams. This allows multiple data streams to be simultaneously transmitted on the same time-frequency slot, and yet interfere in a benign and controlled manner at each desired UT. For instance, when using zero-forcing beamforming (ZFBF) [36], knowledge of the channel matrix can be exploited in order to precode the data such that each UT receives only its intended data symbol, and all other interfering streams from the same AP cancel out (see Section IV-D for more details).

#### IV. MODELING OF NEXT GENERATION WIRELESS

##### A. Common System Level Parameters

**Frequency Reuse/Channel Assignment.** In our numerical examples, we have assumed that the system has 80 MHz of total bandwidth that can be partitioned into 20 MHz or 40 MHz non-overlapping channels or a single 80 MHz channel, with reference to the 802.11 2.4GHz band and the 802.11ac revision [37]. Each AP is active on one of the system channels. The same orthogonal channel can be allocated to multiple APs according to some suitable spatial frequency reuse scheme. The allocation of channels to APs is, in general, a hard problem. In this work, we have adopted a one-pass, greedy algorithm. APs are ordered according to a random sorting permutation  $\pi$  and choose their channel sequentially, such that AP  $\pi(i)$  makes its choice at step  $i$  and chooses channel  $c_{\pi(i)} \in \mathcal{C}$  where  $\mathcal{C}$  is the set of available (non-overlapping) system channels (numbered as  $1 \dots |\mathcal{C}|$ ). The channel choice is made according to the rule:

$$c_{\pi(i)} = \arg \min_{c \in \mathcal{C}} \left\{ \sum_{j < i: \pi(j) \in \mathcal{A}_c(i)} I_{\pi(i), \pi(j)}^c \right\}$$

where  $I_{\ell, r}^c$  denotes the interference power received by AP  $\ell$  from AP  $r$  in channel  $c$ , and  $\mathcal{A}_c(i)$  denotes the set of APs already assigned to channel  $c$  at step  $i$  of the assignment procedure.

**User-AP Association.** The simplest, most widely used user-AP association algorithm connects each user to the AP with the highest Received Signal Strength Indication (RSSI). This approach does not take into account load balancing since in the presence of a non-uniform user spatial distribution, some APs may be cluttered by a lot of users while other APs may be left almost idle. The typical industry solution to this problem is to “force” a new user to switch to another AP if the AP with the strongest RSSI has already too many users, and support client roaming between APs when conditions change [1].

The AP association and load balancing issue are relatively well-studied problems in academia, see, for example, [15], [17], [38]. In our examples (see Section VI), we have considered a heuristic user-AP assignment scheme aimed at

improving the system fairness. Inspired by the work in [39], we allocate users based on “available capacity.” A central controller orders the users according to a sorting random permutation  $\pi'$  and associate each user sequentially to the AP that offers the largest available capacity. In particular, the association algorithm starts by assigning to all APs  $i = 1, \dots, N_a$  an empty set  $\mathcal{S}_i = \emptyset$  of associated users. Then, at step  $k$ , user  $\pi'(k)$  is added to the set  $\mathcal{S}_{i_k}$  if  $i_k$  is the AP index satisfying

$$i_k = \arg \max_{i=1, \dots, N_a} \frac{C_{i, \pi'(k)}}{|\mathcal{S}_i \cup \{\pi'(k)\}|},$$

where  $C_{i,k}$  denotes the peak rate of the link from AP  $i$  to user  $k$ . The association ends when all users have been assigned. Notice that we use the ratio  $\frac{C_{i, \pi'(k)}}{|\mathcal{S}_i \cup \{\pi'(k)\}|}$  as a proxy of the *average* throughput that user  $\pi'(k)$  can get from AP  $i$ . This is motivated by the fact that, under proportional fairness scheduling, each AP allocates its downlink channel resource in equal proportion to its associated users (equal air time policy).

Note that while the channel allocation and user-AP association schemes adopted in this paper are sensible approaches, they do not correspond necessarily to optimal strategies. Nevertheless, the purpose of this paper is not that of proposing system optimization strategies, rather, our focus is to develop a general analytical model which works irrespectively of the specific channel allocation and user-AP association scheme and can be used to enable such type of system optimization.

## B. CSMA Modeling

In order to model CSMA, we focus on the downlink and assume that only APs compete with each other for the wireless medium. The APs form a contention graph by setting an SINR threshold below which the AP-to-AP interference is treated as noise. (This is known as the Clear Channel Assessment (CCA) threshold.) APs in the sensing range of each other that operate on the same channel cannot operate simultaneously, due to the CSMA/CA algorithm and thus they share a link in the contention graph.

We start with an idealized 802.11 CSMA model as in [21]–[24]. Since our goal is to deduce an analytically tractable yet reasonably accurate model (see Section V for a validation of the model against NS-2 simulations [40]), we assume that the transmission and countdown times are exponentially distributed with means  $1/\mu$  and  $1/\lambda$  respectively, and the medium can be sensed instantaneously, thus collisions between APs can be avoided. The first assumption makes the system easy to analyze since it can be modeled as a Continuous Time Markov Chain (CTMC) and can be relaxed to milder and more natural system assumptions without significantly affecting the results, as shown in [22]. The second assumption might lead to an overestimation of the throughput of CSMA when the system spends a sizable time in collisions. However, in practical and well-designed topologies, as in optimized enterprise WiFi networks, this is not the case. It is important to note that our CSMA model operates on top of an SINR-based PHY model and thus we fully model phenomena like hidden terminals, channel capture, etc.

The states of the aforementioned CTMC are all the different feasible transmission patterns for the  $N_a$  APs (that is, only

non-conflicting APs, or, equivalently, independent sets of APs, can transmit at the same time) and the transitions between the different states happen when an AP that is not conflicting with the APs currently transmitting, gets out of countdown and starts transmitting, or when an AP finishes its transmission. Let  $\mathbf{m} = \{m_k | k = 1, \dots, N_a\}$  be the binary state vector of the CTMC, where we let  $m_i = 1$  if AP  $i$  is transmitting and  $m_i = 0$  otherwise. Let  $\mathcal{M} \subseteq \{0, 1\}^{N_a}$  be the state space of the CTMC (independent sets of the interference conflict graph). It can be shown that the limiting stationary distribution of state  $\mathbf{m} \in \mathcal{M}$  is given by:

$$\pi_{\mathbf{m}} = \frac{\rho^{\|\mathbf{m}\|_1}}{\sum_{\mathbf{m}' \in \mathcal{M}} \rho^{\|\mathbf{m}'\|_1}}, \quad (2)$$

where  $\rho = \lambda/\mu$  and  $\|\cdot\|_1$  is the  $\mathbf{L}_1$  norm, thus  $\|\mathbf{m}\|_1$  is the number of APs transmitting during state  $\mathbf{m}$ .

As an example, in Figure 1a we see 6 APs operating on the same channel and the corresponding contention graph. There are 13 feasible states for this graph and the probabilities for each state can be seen in Figure 1b. Intuitively, one expects that larger independent sets are more likely to be scheduled by CSMA, since once an AP is selected, all sets not containing this AP will not be scheduled. Indeed, the probabilities in Figure 1a are a lot larger for larger independent sets because the transmission times are a lot larger than the countdown times and thus  $\rho \gg 1$ . As a result, in large networks it is reasonable to take into account only states corresponding to *maximal independent sets* of the interference graph, rather than all feasible states. It should be noted here that identifying the maximal independent sets of a graph is known to be an NP-complete problem, nevertheless given the specific characteristics of each topology (AP density, symmetric placement etc) we have successfully run large examples in a few minutes.

Having computed the fraction of time that the network spends in each transmission pattern  $\mathbf{m} \in \mathcal{M}$ , we next take into account the throughput resulting from CSMA/CA. To do so, we evaluate the total spectral efficiency (or each individual UT spectral efficiency) achieved for each transmission pattern as shown in the rest of the section, average these values with respect to the stationary distribution (see Equation 2), and multiply the result by the channel bandwidth to obtain the throughput in bit/s.

## C. Single-user Beamforming

**User rates with single-user beamforming.** Without loss of generality, let AP  $i$  be active on channel  $c_i$ , and let  $\nu = 1, \dots, N$  denotes the corresponding OFDM subcarriers. Assume that UT  $k$  is associated with AP  $i$ , i.e.,  $k \in \mathcal{S}_i$ . The *instantaneous peak rate* at which AP  $i$  can serve user  $k$  is given by

$$C_{ik}^{\mathbf{m}} = m_i \frac{1}{N} \sum_{\nu=1}^N \log(1 + \text{SINR}_{ik}^{\mathbf{m}}[\nu]), \quad (3)$$

where  $\mathbf{m}$  denote the current state of the CMTMC (such that this rate is zero if  $m_i = 0$ , i.e., AP  $i$  is not in the current active set according to the CSMA protocol). The rate  $C_{ik}^{\mathbf{m}}$  is measured in bit/s/Hz, and it is referred to as “instantaneous” since it is a

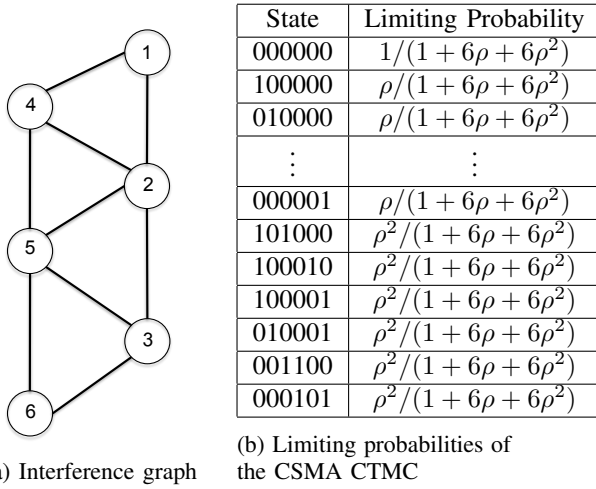


Fig. 1: AP interference graph and limiting probabilities of the corresponding CSMA CTMC.

function of the realization of the fading channel coefficients. The term  $\text{SINR}_{ik}^m[\nu]$  denotes the Signal to Interference plus Noise Ratio on subcarrier  $\nu$ . With single-user beamforming, this is given by

$$\text{SINR}_{ik}^m[\nu] = \frac{g_{ik} \|\mathbf{h}_{ik}[\nu]\|^2 P_i}{1 + \sum_{j \in \mathcal{A}_{c_i}: j \neq i} m_j g_{jk} |\mathbf{v}_j^H[\nu] \mathbf{h}_{jk}[\nu]|^2 P_j}, \quad (4)$$

where, as defined before, the set  $\mathcal{A}_{c_i}$  includes the APs assigned to channel  $c_i$ ,  $P_i$  denotes transmit power spectral density (energy per frequency domain symbol) of AP  $i$  and  $\mathbf{v}_i[\nu] = \mathbf{h}_{ik}[\nu]/\|\mathbf{h}_{ik}[\nu]\|$  is the unit-norm transmit beamforming vector of AP  $i$  serving user  $k$ , according to the conjugate beamforming scheme (see Section III). The interfering AP  $j \in \mathcal{A}_{c_i}$  uses the same scheme, with a unit vector  $\mathbf{v}_j[\nu]$  that depends on the channel vector to its own intended user. In the SINR denominator, the inner product  $\mathbf{v}_j^H[\nu] \mathbf{h}_{jk}[\nu]$  corresponds to the ‘‘spatial coupling’’ between such vector and the channel vector from AP  $j$  and user  $k$ . It is important to notice that  $\mathbf{v}_j[\nu]$  and  $\mathbf{h}_{jk}[\nu]$  are statistically independent. Instead, the coupling between the beamforming vector  $\mathbf{v}_i[\nu]$  of AP  $i$  and its intended user channel  $\mathbf{h}_{ik}[\nu]$  yields  $\mathbf{v}_i^H[\nu] \mathbf{h}_{ik}[\nu] = \|\mathbf{h}_{ik}[\nu]\|$  which yields the beamforming gain at the numerator of the SINR. It follows that  $|\mathbf{v}_j^H[\nu] \mathbf{h}_{jk}[\nu]|^2$  is a chi-squared random variable with 2 degrees of freedom, while  $\|\mathbf{h}_{ik}[\nu]\|^2$  is a chi-squared random variable with  $2M$  degrees of freedom.

In order to obtain simple deterministic analytical formulas for the rates, we consider that  $M$  is large enough such that the effect of small-scale fading disappears. Hence,  $\|\mathbf{h}_{ik}[\nu]\|^2 \rightarrow M$  (beamforming gain equal to the number of antennas per AP), and  $|\mathbf{v}_j^H[\nu] \mathbf{h}_{jk}[\nu]|^2 \rightarrow 1$ . The resulting approximated deterministic rate formula for the peak rate is:

$$C_{ik}^m = m_i \log \left( 1 + \frac{g_{ik} M P_i}{1 + \sum_{j \in \mathcal{A}_{c_i}: j \neq i} m_j g_{jk} P_j} \right).$$

With orthogonal downlink multiple access (TDMA) the rate region for the downlink of AP  $i$  for  $m_i = 1$  (i.e., in the time slots where AP  $i$  is allowed to transmit because of CSMA/CA)

is given by the set of non-negative rates  $\{R_{ik}^m : k \in \mathcal{S}_i\}$  such that

$$\sum_{k \in \mathcal{S}_i} \frac{R_{ik}^m}{C_{ik}^m} \leq 1. \quad (5)$$

With proportional fairness downlink resource allocation, the system operates at the rate point

$$R_{ik}^m = \frac{m_i}{|\mathcal{S}_i|} \log \left( 1 + \frac{g_{ik} M P_i}{1 + \sum_{j \in \mathcal{A}_{c_i}: j \neq i} g_{jk} P_j} \right). \quad (6)$$

Eventually, the average spectral efficiency of user  $k \in \mathcal{S}_i$  when also averaging with respect to the stationary distribution of the CTMC that describes the CSMA/CA MAC layer, is given by

$$R_{ik} = \sum_{\mathbf{m} \in \mathcal{M}} \pi_{\mathbf{m}} \cdot R_{ik}^m. \quad (7)$$

In order to convert this number in the more usual average throughput in bit/s, it is sufficient to multiply  $R_{ik}$  by the channel bandwidth  $W_{c_i}$  (measured in Hz) of the channel  $c_i$  allocated to AP  $i$ .

Once the user spectral efficiencies  $R_{ik}$  are determined, we can present the results in terms of the throughput CDF for a given placement of the APs and of the UTs, pathloss realization, channel allocation and user-AP association. Letting  $T_{ik} = W_{c_i} R_{ik}$  denote user  $k$  average throughput in bit/s, the throughput CDF over the user population is given by

$$F_T(r) = \frac{1}{\sum_i |\mathcal{S}_i|} \sum_{i,k} 1 \{T_{ik} \leq r\}. \quad (8)$$

It follows that  $F_T(r)$  indicates the fraction of users with throughput less or equal to some number  $r$ .

#### D. Concentrated MU-MIMO

We now consider the case where each AP  $i$  implements MU-MIMO in order to serve its associated users  $k \in \mathcal{S}_i$ . This scheme is inspired by the MU-MIMO mode of 802.11ac [37]. We denote this scheme as ‘‘concentrated’’ MU-MIMO in order to stress the difference with respect to a distributed MU-MIMO approach that shall be treated in the next section, and may be regarded as a future trend of WLANs and small cell networks. The main difficulty here is represented by the fact that AP  $i$  can simultaneously serve a subset of users of size not larger than  $\min\{M, |\mathcal{S}_i|\}$ . Consistent with the 802.11ac standard [37], we consider MU-MIMO based on ZFBF.

Let  $\hat{\mathcal{S}}_i \subseteq \mathcal{S}_i$  denote the subset of users to be served on a given time slot in MU-MIMO mode, and let  $S_i = |\hat{\mathcal{S}}_i|$  indicate its size. The  $M \times 1$  channels of users  $k \in \hat{\mathcal{S}}_i$  are assumed to be known at the AP  $i$  transmitter through some form of channel state feedback (e.g., as specified in the 802.11ac standard). Such channel vectors are collected as the columns of a  $M \times S_i$  channel matrix  $\mathbf{H}_i[\nu] = [\mathbf{h}_{i1}[\nu], \dots, \mathbf{h}_{iS_i}[\nu]]$ , for all the subcarriers  $\nu$  forming channel  $c_i$ , as defined before. The ZFBF precoded signal vector on subcarrier  $\nu$  is given by  $\mathbf{x}_i[\nu] = \mathbf{V}_i[\nu] \mathbf{u}_i[\nu]$ , where  $\mathbf{u}_i[\nu]$  is a  $S_i \times 1$  columns vector of frequency-domain coded modulation symbols to be sent to users  $k \in \hat{\mathcal{S}}_i$  and  $\mathbf{V}_i[\nu]$  is the ZFBF precoding matrix, of dimension  $M \times S_i$ . Following [36], this is given by

$$\mathbf{V}_i[\nu] = \mathbf{H}_i[\nu] (\mathbf{H}_i^H[\nu] \mathbf{H}_i[\nu])^{-1} \boldsymbol{\Xi}_i^{1/2}[\nu] \quad (9)$$

where  $\Xi_i[\nu]$  is a column-normalizing diagonal matrix included in order to preserve the total AP transmit power. In particular, the  $k$ -th diagonal element of  $\Xi_i[\nu]$  is given by

$$\xi_{ik}[\nu] = \frac{1}{\left[ (\mathbf{H}_i^H[\nu] \mathbf{H}_i[\nu])^{-1} \right]_{kk}}$$

where  $[\cdot]_{kk}$  denotes the  $k$ -th diagonal element of the matrix argument. Using the fact that  $\mathbf{V}_i^H[\nu] \mathbf{H}_i[\nu] = \Xi_i^{1/2}[\nu]$  and letting  $\lambda_{ik}[\nu] = g_{ik} \xi_{ik}[\nu]$  denote the effective channel coefficient including also the effect of the large-scale gain, from Equation (1), the signal received at UT  $k$  takes on the form

$$\begin{aligned} y_k[\nu] &= \sqrt{g_{ik}} \mathbf{u}_i[\nu]^H \mathbf{V}_i^H[\nu] \mathbf{h}_{ik}[\nu] + z_k[\nu] \\ &= \sqrt{\lambda_{ik}[\nu]} u_{ik}[\nu] + z_k[\nu], \end{aligned} \quad (10)$$

where it is apparent that the multi-access interference from signals generated by AP  $i$  and sent to the other users  $k' \in \widehat{\mathcal{S}}_i$  with  $k' \neq k$  is completely eliminated by ZFBF precoding.

**User rates with ZFBF.** Based on the effective channel (10), we have that the instantaneous user rate takes on the same form (3) with a different expression of  $\text{SINR}_{ik}^m[\nu]$ . In particular, in the case of concentrated MU-MIMO with ZFBF precoding this is given by

$$\text{SINR}_{ik}^m[\nu] = \frac{\lambda_{ik}[\nu] P_i / S_i}{1 + \sum_{j \in \mathcal{A}_{c_i}; j \neq i} m_j g_{jk} \|\mathbf{V}_j^H[\nu] \mathbf{h}_{jk}[\nu]\|^2 P_j / S_j}, \quad (11)$$

where we have assumed (for the sake of simplicity) uniform power allocation over the downlink data streams, i.e., each user gets  $1/S_i$  of the total AP transmit power.

A major difficulty here is represented by the fact that the coefficient  $\lambda_{ik}[\nu]$  depends on the channel matrix through the whole selected group of users  $\widehat{\mathcal{S}}_i$ , which means that the individual user rates do not “decouple”: for finite dimension, we need to calculate the rates for all the  $G_i = \binom{|\mathcal{S}_i|}{S_i}$  possible groups. In order to alleviate this problem and obtain a “decoupled” rate expression, we resort to asymptotic formulas. Inspired by prior work of ours [5], we consider the regime where both  $M$  and  $S_i$  become large while keeping the ratio  $S_i/M \leq 1$  and fixed. Specifically, we scale all channel coefficients by  $1/\sqrt{M}$  and multiply the transmit power by a factor  $M$ , which yields

$$\lambda_{ik}[\nu] \rightarrow \left(1 - \frac{S_i - 1}{M}\right) g_{ik},$$

and

$$\|\mathbf{V}_j^H[\nu] \mathbf{h}_{jk}[\nu]\|^2 \rightarrow \frac{1}{M} \text{tr}(\mathbf{V}_j^H[\nu] \mathbf{V}_j[\nu]) = \frac{S_j}{M}.$$

With these limits, we obtain the SINR deterministic approximation (which becomes exact in the large-system regime)

$$\text{SINR}_{ik}^m \rightarrow \frac{(M - S_i + 1) g_{ik} P_i / S_i}{1 + \sum_{j \in \mathcal{A}_{c_i}; j \neq i} m_j g_{jk} P_j}. \quad (12)$$

Notice that, as in the case of single-user beamforming, this limit does not depend on the subcarrier index  $\nu$  any longer. Also, for the sake of consistency, it is interesting to notice that for  $S_i = 1$  we recover the expression for single user conjugate beamforming in Equation (4).

Under this approximation, the vector of user rates for a given active group of users  $\widehat{\mathcal{S}}_i \subseteq \mathcal{S}_i$  is given by

$$C_{ik}^m(\widehat{\mathcal{S}}_i) = \begin{cases} 0 & \text{for } k \in \mathcal{S}_i - \widehat{\mathcal{S}}_i \\ m_i \log(1 + \text{SINR}_{ik}^m) & \text{for } k \in \widehat{\mathcal{S}}_i. \end{cases} \quad (13)$$

**Rate region for concentrated MU-MIMO.** The achievable rate region in the case of concentrated MU-MIMO is significantly more complicated to express than for the case of single-user beamforming with downlink orthogonal access. In this case, any group of users  $\widehat{\mathcal{S}}_i \subseteq \mathcal{S}_i$  with size  $S_i \leq M$  can be scheduled in the downlink. The individual average rate of user  $k$  is the convex combination of the rates achieved in each group, where the convex combination coefficients depend on the downlink scheduling scheme. In particular, we can order the groups  $\widehat{\mathcal{S}}_i \subseteq \mathcal{S}_i$  of size  $S_i \leq M$  in lexicographic order. Let  $\mathbf{C}_i^m(\widehat{\mathcal{S}}_i)$  denote the  $1 \times |\mathcal{S}_i|$  row vector of user rates given in (13), and let  $\mathbf{C}^m(\mathcal{S}_i)$  denote the  $G_i \times |\mathcal{S}_i|$  matrix obtained by stacking all the group rate rows on top of each other in the same group lexicographic order. Define the  $1 \times |\mathcal{S}_i|$  rate vectors  $\mathbf{R}_i^m$  with components  $R_{ik}^m$  for all users  $k \in \mathcal{S}_i$ . The rate region obtained by applying TDMA downlink scheduling on top of MU-MIMO for each AP  $i$  is given by the union of all points  $\mathbf{R}_i^m$  satisfying

$$\mathbf{R}_i^m \leq \boldsymbol{\rho}^\top \mathbf{C}^m(\mathcal{S}_i) \quad (14)$$

for some non-negative time-sharing vector  $\boldsymbol{\rho}$  of dimension  $G_i \times 1$ , with components satisfying  $\sum_{k \in \mathcal{S}_i} \rho_k = 1$ . Notice also that this region generalizes the single-user beamforming TDMA region given in (5), since in this case we have only  $|\mathcal{S}_i|$  possible groups of size 1, and combining the inequalities

$$R_{ik}^m \leq \rho_k C_{ik}^m$$

with  $\sum_{k \in \mathcal{S}_i} \rho_k = 1$  yields again Equation (5).

Focusing on proportional fairness downlink resource allocation, the AP gives to each user  $k \in \mathcal{S}_i$  equal air time, such that the user rates are given by

$$R_{ik}^m = m_i \frac{S_i}{|\mathcal{S}_i|} \log(1 + \text{SINR}_{ik}^m). \quad (15)$$

The number of downlink streams  $S_i$  may be fixed by some technology constraints (e.g., by the number of data streams that the AP chipset is able to precode), or it may be optimized for each AP, subject to the constraint  $S_i \leq \min\{M, |\mathcal{S}_i|\}$ . In this work, the latter was chosen as we maximize the sum-rate that every AP serves its users individually for every AP.

As before, the average user rate over all possible states of the CSMA/CA CTMC is given by using Equation (15) in (7). From the resulting average rates  $\{R_{ik}^m\}$ , the throughput CDF can be obtained via Equation (8).

### E. Distributed MU-MIMO

In this case we assume that all APs that operate in the same channel cooperate and act as a single virtual mega AP (no contention between the APs for the wireless medium). Therefore, the channel index is not necessary and is dropped for notation simplicity.

Assume that  $B$  APs with  $M$  antennas each form a cluster, pooling together all their  $BM$  antennas, and collectively serve the population of  $K$  UTs with a single antenna each. This type of distributed MU-MIMO configuration has been widely studied as far as the PHY algorithms and the achievable rates from a communication theoretic viewpoint are concerned (see for example prior work of ours [5], [6], [31] and others [11], [41]). Recently, experimental results with such systems have been published (see for example our own prior work [3] as well as work from others [4], [42]). As before, we wish to characterize the rate per user in which a subset  $\hat{\mathcal{S}}$  of size  $S < \min\{K, BM\}$  of users is served simultaneously by the distributed MU-MIMO scheme. We shall then apply a TDMA scheduling over the user subsets in order to obtain a desired throughput  $K$ -tuple satisfying some required fairness criterion.

As far as the PHY schemes and corresponding performance are concerned, the analysis of distributed MU-MIMO is significantly more involved than the previously treated cases because the channel vectors from all the AP antennas to any given user are not i.i.d. given the pathloss. In fact, letting  $g_{ik}$  denote again the channel gain coefficient from AP  $i$  to user  $k$  and letting  $\mathbf{h}_{ik}[\nu]$  denote the channel small fading coefficient, we have that the composite channel vector is given by

$$\mathbf{h}_k[\nu] = \begin{bmatrix} \sqrt{g_{1k}}\mathbf{h}_{1k}[\nu] \\ \sqrt{g_{2k}}\mathbf{h}_{2k}[\nu] \\ \vdots \\ \sqrt{g_{Bk}}\mathbf{h}_{Bk}[\nu] \end{bmatrix}.$$

For a certain set of  $\hat{\mathcal{S}} = \{1, \dots, S\}$  users to be served, the resulting  $BM \times S$  channel matrix takes on the form

$$\mathbf{H}[\nu] = \begin{bmatrix} \sqrt{g_{11}}\mathbf{h}_{11}[\nu] & \sqrt{g_{12}}\mathbf{h}_{12}[\nu] & \cdots & \sqrt{g_{1S}}\mathbf{h}_{1S}[\nu] \\ \sqrt{g_{21}}\mathbf{h}_{21}[\nu] & \sqrt{g_{22}}\mathbf{h}_{22}[\nu] & \cdots & \sqrt{g_{2S}}\mathbf{h}_{2S}[\nu] \\ \vdots & \vdots & \ddots & \vdots \\ \sqrt{g_{B1}}\mathbf{h}_{B1}[\nu] & \sqrt{g_{B2}}\mathbf{h}_{B2}[\nu] & \cdots & \sqrt{g_{BS}}\mathbf{h}_{BS}[\nu] \end{bmatrix}$$

where the effective channel coefficient  $\lambda_k$  and the SINR for user  $k \in \hat{\mathcal{S}}$  under joint ZFBF from all the  $B$  APs are given by

$$\lambda_k[\nu] = \frac{1}{\left[ (\mathbf{H}^H[\nu]\mathbf{H}[\nu])^{-1} \right]_{k,k}}, \quad \text{SINR}_k[\nu] = \lambda_k[\nu] \frac{P_{\text{sum}}}{S}, \quad (16)$$

where we define the sum power of all APs in the cluster as  $P_{\text{sum}} = \sum_{i=1}^B P_i$  and assume equal power allocation on all downlink data streams. Note that since all APs operate as a single virtual mega AP, there is no interference between APs and thus there is no interference term in the SINR above.

The problem is that now the structure of the channel matrix depends on the actual set of users  $\hat{\mathcal{S}}$  being served. Hence, even using asymptotic formulas from random matrix theory, we should evaluate rates for each set of  $\binom{K}{S}$  users, for  $S = 1, \dots, \min\{K, BM\}$ . With distributed MU-MIMO, relevant numbers are (for example)  $K = 100$ ,  $M = 4$  and  $B = 16$ . Clearly even enumerating all the possible active user subsets  $\hat{\mathcal{S}}$  is difficult.

Inspired by prior work of ours [5] we propose the following simplification: Under certain symmetry conditions in the

pathloss coefficients, the effective channel coefficient  $\lambda_k[\nu]$  for user  $k$  under joint ZFBF from all the  $B$  APs, in the limit for large  $M$  and large  $S$  with fixed ratio  $M/S$ , asymptotically takes on the form:

$$\lambda_k[\nu] \rightarrow \left( 1 - \frac{S-1}{BM} \right) \left( \sum_{i=1}^B g_{ik} \right).$$

Once more, the limiting expression does not depend on the subcarrier index any longer. We use the above expression as an approximation of the ZFBF effective channel coefficients for general distributed MU-MIMO. This has the following appealing interpretation: the distributed MU-MIMO scheme behaves as a concentrated MIMO system with pathloss coefficients equal to the sum of the pathloss coefficients and the total number of antennas (the number of antennas of all coordinated APs in the cluster). Thus, we obtain the (approximated) user downlink rate as:

$$C_k = \begin{cases} 0, & k \in \mathcal{S} - \hat{\mathcal{S}} \\ \log \left( 1 + \left( M - \frac{S-1}{B} \right) \left( \sum_{i=1}^B g_{ik} \right) \frac{P_{\text{sum}}}{S} \right), & k \in \hat{\mathcal{S}} \end{cases} \quad (17)$$

Notice that this is the effective performance of a virtual concentrated MU-MIMO system with ‘‘resource pooling’’, with  $M$  effective antennas, effective load (number of active users per antenna) equal to  $S/B$ , effective channel gains  $g_k = \sum_{i=1}^B g_{ik}$  and effective power  $P_{\text{sum}}$ . Notice also that for  $B = 1$  the above formula coincides with the case developed for concentrated MU-MIMO in the absence of inter-AP interference.

For a network with  $N_a$  APs, letting  $B = N_a$  with distributed MU-MIMO yields that the whole network corresponds to a single coordination cluster. In practice, this may be too constraining since other system limitation aspects arise in distributed MU-MIMO architectures. For example, since all user data need to be precoded jointly from all the coordinated APs in the cluster, eventually the wired backbone network connecting the APs will become the system bottleneck. Here we are not concerned with such practical implementation problems of distributed MU-MIMO, but for the sake of generality we wish to take into account the case where the network is split into multiple coordination clusters. In particular, in some numerical results we consider the case where the network is split into 4 clusters, each of which with  $B = N_a/4$  APs, and operating on a different 20 MHz channel, such that there is no inter-cluster interference. In this case, the same formula (17) applies, where we restrict the active user set  $\hat{\mathcal{S}}$  to be a subset of the users assigned to the given cluster. Similarly, we can cluster the APs in 2 clusters assigning the two 40 MHz non-overlapping channels to each one. User-cluster association can be done through a greedy scheme similar to what we have seen before for the user-AP association.

As with the single-user beamforming and concentrated MU-MIMO systems, for distributed MU-MIMO we are interested in the per-user downlink throughput under proportional fairness scheduling. Letting  $S$  denote the number of users simultaneously served by the cluster of APs and assuming that users are given equal air time, we have that each user  $k$  is served for a fraction of time equal to  $\frac{S}{K}$ . Hence, the proportional fairness scheduler with equal power per stream

yields throughput

$$R_k = \frac{S}{K} \log \left( 1 + \left( M - \frac{S-1}{B} \right) \left( \sum_{i=1}^B g_{ik} \right) \frac{P_{\text{sum}}}{S} \right). \quad (18)$$

These rates can be maximized with respect to the size of the active user set  $S = 1, 2, \dots, \min\{K, BM\}$ . From the resulting average rates  $\{R_{ik}\}$ , the throughput CDF can be obtained again via Equation (8).

## V. MODEL VALIDATION

We will proceed with the validation of our model in two steps. First, we will evaluate the accuracy of the analytic PHY models using a custom Monte Carlo simulator implemented in Matlab, and then the accuracy of the MAC model (CSMA CTMC) using NS-2 [40]. Notice that no open-source 3rd party simulator supports the advanced PHY layer schemes that we consider, and thus this two step validation process is required to validate our model in its entirety.

As an example, consider Equation (7) which gives the rate of a user under single-user beamforming. This equation uses the rates computed in (6) and the stationary distribution of the CSMA CTMC computed in (2). In the first step of the validation process we will use our custom simulator to verify the accuracy of Equation (6), and, in the second step we will use NS-2 to validate Equation (2). A similar process is used for the cases of concentrated MU-MIMO and distributed MU-MIMO, where in the former case the user rates are given by (15) and in the later by (18).

We start with the first step of the validation process, namely the validation of Equations (6), (15), and (18). In all three cases, we compare the distribution of the average per-user rates as computed by the model and by our simulation for some representative tractable scenarios of interest, namely an open conference hall (see section VI-B) and an office with rooms (see section VI-D). We utilize the same user locations for both the analytic and simulation results, which are illustrated in Figures 5a and 5c. For the scenarios which require APs to use orthogonal channels, the channel selection is performed as in Section IV-A, where 4 channels of 20MHz each are shared among the APs. Lastly, the user-AP association is performed as in Section IV-A as well.

Our custom Monte Carlo simulator proceeds as follows. For each topology scenario it creates a large number of channel instantiations. Then, for a particular channel realization, it computes the received signal power and the received interference power for each user, calculates the SINR of each user under that channel realization, and computes the corresponding (gaussian) user rates. Finally, it calculates the average achievable rate for each user across all the channel realizations and the empirical distribution of user rates. It is important to note that the instantaneous SINR values are computed using a different formula by the Monte Carlo simulator depending on the PHY model. For single-user beamforming we use (4), for concentrated MU-MIMO (11), and for distributed MU-MIMO (16) (and variations to take into consideration different cluster sizes). Note that these are stochastic formulas which depend on the channel realization and it is for this reason that in Section

IV we obtain simple yet accurate deterministic formulas which form the gist of our analytical model, e.g. Equation (12) in place of (11). Notice also that our deterministic formulas remove other stochastic aspects of the problem as well, like the dependence of user MIMO scheduling in instantaneous SINR values.

For the SU-MISO simulations, each transmitter transmits to a random user located within its cell on each iteration. The transmitters are assumed to have channel state information, so the transmitters beamform to their selected user. Physically adjacent APs operate on separate channels, such that users experience interference only from non-neighbor APs transmitting on the same frequency. Each AP transmits with power  $P = 90\text{dB}$  above the noise floor, and at a bandwidth of 20 MHz. Including pathloss, the users receive their respective signals at typical Wi-Fi SNRs in the range of roughly 0-40dB.

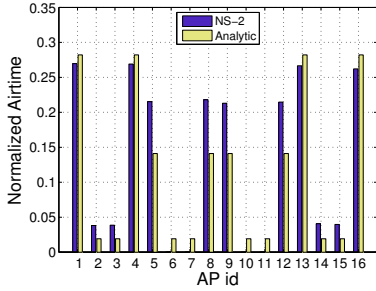
In the case of the 802.11ac-like approach, APs retain the same channel allocation as in the SU-MISO simulations, such that neighboring APs operate on different frequencies. Instead of transmitting to a single user, however, they beamform to a random subset of the users in each cell using ZFBF. Based on simulation trials, we determined the optimal number of users (on average) to serve simultaneously in each cell, which was typically 2 or 3. Again, each AP transmits with power  $P = 90\text{dB}$  above the noise floor at a bandwidth of 20 MHz.

The distributed MIMO simulations utilize a clustering approach in which groups of 5 APs achieve sufficient synchronization such that they act as a single 20-antenna AP. In this case, all interference is nulled within a given cluster, and each cluster is assigned to a channel as in the previous two simulations. We assume that the APs pool their power, such that total transmit power is  $\sim 97\text{dB}$  within each cluster. This simplifies the treatment of the precoder calculation, but it may allow individual APs to transmit higher than 90dB power above the noise floor. In practice, we would need to utilize results on ZFBF under per-antenna power constraints [43], though we avoid this issue since it is not treated in the model. As in the previous simulations, each cluster occupies 20 MHz of bandwidth.

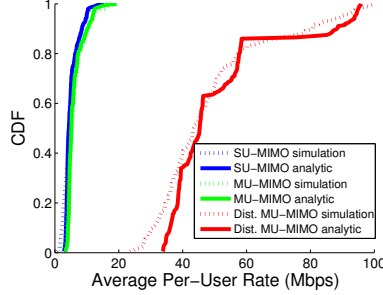
Figures 2b, 2c and 4 display the CDFs of the average per-user rates for the simulations and the models. Although the analytic models make a number of assumptions, for example, in the single-user beamforming case that the number of antennas  $M$  per AP is large, in the concentrated MU-MIMO case that the number of antennas and users per AP is large, and in the distributed MU-MIMO case that, in addition, there is a specific geometric symmetry in the topology, we see that the Monte Carlo simulation results and the analytical results are quite close.

Lastly, we proceed to the second step of the validation process and evaluate the accuracy of the CSMA CTMC model used in this work for the open conference hall scenario depicted in Figure 5a using NS-2 [40]. In order to infer the APs' relative airtime in NS-2, an 802.11 scenario was constructed where every AP was transmitting a UDP stream with constant bit rate (CBR) traffic of 7 Mbps to a closely located UT. The basic rate was set to 1 Mbps, the data rate to 11 Mbps, the capture future was turned of and the

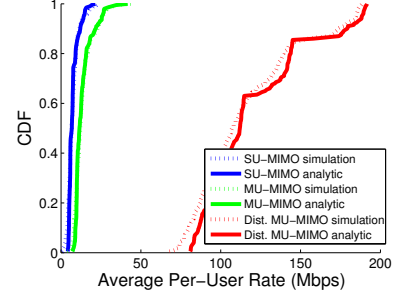




(a) NS-2 and analytic relative airtime allocations over 16 APs.



(b) 20 APs and 4 antennas per AP



(c) 20 APs and 10 antennas per AP

Fig. 2: CDFs and NS-2 results of the avg. user rate for the analytic model vs. simulation for the conference hall scenario.

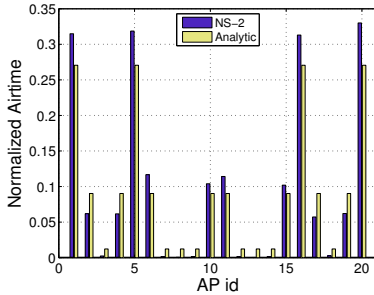
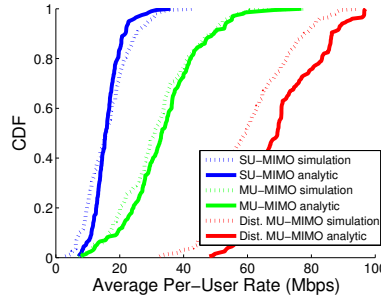
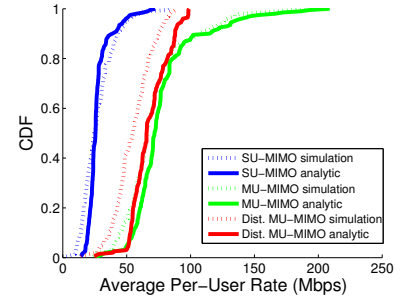


Fig. 3: NS-2 and analytic relative airtime allocations over 20 APs.



(a) 4 rooms, 20 APs, 4 antennas per AP



(b) 40 rooms, 20 APs, 4 antennas per AP

Fig. 4: CDFs of the avg. user rate for the analytic model vs. simulation for the office floor scenario.

carrier sensing and receiving thresholds were arranged so that the same interference landscape was created for both the simulation and the CTMC model. Every AP in isolation could transmit at a rate of 4.97 Mbps, and thus, by simulating the achievable throughput when all APs were transmitting, we can estimate the relative airtime of each AP. The results can be seen in Figures 2a and 3 for 16 and 20 APs respectively. Note that a similar CTMC CSMA model has been validated under small scale scenarios in [22].

## VI. RESULTS

In the following section, results and insights from the application of the analytic model in various practical scenarios will be presented.

### A. OFDM and MCS overhead

We discuss the rate degradation from having actual quantized rates based on the 802.11 standard's Modulation and Coding schemes (MCS) along with the overhead incurred by OFDM. There are of course other sources of overhead as well, e.g. the CSMA overhead which been included in our model already (see Section IV-B), and the overhead to collect channel state information and/or coordinate remote APs in the context of distributed MU-MIMO which will be discussed later (see Section VI-F).

Starting from the OFDM overhead we note that based on the 802.11ac standard [37] for channels of 20 MHz bandwidth,

only 52 of the 64 subcarriers carry data (the rest are devoted to pilots or are nulled). For 40MHz and 80MHz channels the corresponding numbers are 108 out of 128 subcarriers, and 234 out of 256 subcarriers respectively (notice that these overheads slightly vary for 802.11n and 802.11ac, the numbers of the latter are adopted for reasons of simplicity). Finally, the OFDM Cyclic Prefix (CP) is included in the Guard Interval (GI) that is prepended to every OFDM symbol for a total overhead of an extra 20% (assuming a normal GI of  $0.8 \mu\text{s}$  with total symbol duration of  $4 \mu\text{s}$ ).

As a more realistic approach to the rate calculation, we map the received SINRs into a discrete set of modulation and coding pairs. While we acknowledge that choosing the best among several discrete modulation and coding options (known as rate adaptation) is non-trivial, for the sake of simplicity we assume that we can choose the best scheme based on the received SINR. Table I provides one such mapping that corresponds to the 9 mandatory MCSs of 802.11ac [37], keeping in mind that mappings vary by vendor or may be dynamically chosen in practical scenarios.

The scenarios presented in the rest of the section cover typical yet interesting cases of WiFi deployments, along with more challenging situations. Specifically: i) a densely populated conference hall, ii) an open-floor plan office space, iii) an office building floor with separated rooms and iv) an event stadium with high capacity. For all scenarios 4 antennas per AP are assumed (the maximum number allowed by the 802.11n standard and supported by 802.11ac implementations to date)

802.11ac MCS Index	Modulation	Code Rate	SNR
0	BPSK	1/2	$\geq 2$ dB
1	QPSK	1/2	$\geq 5$ dB
2	QPSK	3/4	$\geq 8$ dB
3	16-QAM	1/2	$\geq 12$ dB
4	16-QAM	3/4	$\geq 15$ dB
5	64-QAM	2/3	$\geq 18$ dB
6	64-QAM	3/4	$\geq 21$ dB
7	64-QAM	5/6	$\geq 24$ dB
8	256-QAM	3/4	$\geq 27$ dB

TABLE I: Modulation/Coding pairs from IEEE 802.11ac and the corresponding SINRs at which they can be selected.

and the user receivers are equipped with 1 antenna, as is the typical case for handheld devices.

### B. Conference Hall

A conference hall of dimension 20mx20m with 200 users and a varying number of APs (see Figure 5a) is examined. Figure 6a plots the average throughput per user against the number of APs. It is obvious that in this scenario, a coordinated solution where interference is suppressed through the distributed MU-MIMO system is highly favorable. As the number of APs increases, the average user throughput increases for the distributed MU-MIMO technology. The greatest gains come if we utilize the whole bandwidth as a single channel and let both APs and user receivers transmit and receive in the whole 80MHz band. Nevertheless, even in the case where we cluster neighboring APs to act as a single AP, assign a 20MHz channel to each cluster, and assign each user to a single cluster (see Section IV-E) the gains are still enormous compared to the non-coordinated technologies.

It is notable that even under the idealized CSMA scenario where collisions are assumed to be insignificant, the throughputs of 802.11n SU-MISO and 802.11ac MU-MIMO are quickly saturated. Thus, increasing the number of APs does not provide any extra gains as can be seen in Figure 6b. Also, the small gains in the figure that different channelization options provide to non-coordinated systems under a strict CCA threshold are due to the reduced OFDM overheads when a smaller number of larger channels is used (see Section VI-A). Notice that this is only true under the assumption of no collisions for the idealized CSMA model. If collisions are taken into account frequency re-use has a greater impact on the throughput.

**CSMA impact as number of APs increases:** In Figures 6b and 6c we see the average per user throughput for different channelization options for the case of CSMA with the default CCA threshold of 10dB above the noise floor and an unbounded CCA threshold (no CSMA present). It is worth to notice that 802.11ac MU-MIMO, being more susceptible to interference, performs significantly worse under the regime of no CSMA. It performs similar to 802.11n's robust conjugate beamforming gains as the number of interferers grows (Figure 6c). Indeed, in this interference limited regime, the MU-MIMO system selects only one user to be served at a time, reverting to a SU-MISO scheme. On the other hand, as can be seen

in Figure 6b, using CSMA random access clearly benefits the MU-MIMO scheme as the multiplexing gains are larger.

**CCA Threshold and Power Control:** Figures 7a and 7b show the change in the average user throughput as power increases and the CCA (Clear Channel Assessment) threshold is changed for 802.11n SU-MISO and 802.11ac MU-MIMO. For this optimization, Gaussian rates have been assumed instead of the discretized rate allocation we introduced. Also, a 4 channel system with 20 MHz per channel and 20 APs serving 200 users is assumed for these computations. We can see from these plots that SU-MISO is more robust to interference as the power of all APs increases, whereas for MU-MIMO to perform with a noticeable multiplexing gain a lower CCA threshold has to be chosen. In Figure 7c we see the optimal CCA threshold for a range of transmit powers from 60 to 120 dB for the two non-coordinated technologies. Notice that thanks to the model we have introduced, such an optimization can be quickly performed and trade-offs can be efficiently explored.

**Sectorization gains:** In the previous results we saw that the distributed MU-MIMO technology significantly outperforms the presented non-coordinated schemes that quickly become interference limited as the number of APs grows. To mitigate the interference between APs that operate on the same channel we can use a *sectorized* deployment. Such deployments can commonly be found in cellular networks, where the antennas used have a sub-circular sector shaped radiation pattern [44], and simplified variations are slowly making their appearance in enterprise WiFi deployments. We present here a simple scheme to illustrate the gains of mitigating the interference for non-coordinated technologies with such an approach. We shape the radiation patterns of all APs in the conference hall topology (Figure 5a) such that they only radiate energy to a  $90^\circ$  sector, oriented towards the same direction for all APs. This simple approach significantly improves the performance of SU-MIMO 802.11n and MU-MIMO 802.11ac technologies as can be seen in Figure 8, by a factor of 3x and 7x respectively. Note that distributed MU-MIMO, which uses omnidirectional antennas, still performs significantly better, especially in a 1 cluster setup. (Only the 4 cluster setup is shown in this plot to better distinguish the performance of the other schemes).

### C. Open-floor office building

The open-floor office scenario shares a few common characteristics with the conference hall but has some interesting differences. We define an office floor of dimensions  $160\text{m} \times 23\text{m}$  that is occupied by cubicles (essentially no walls obscure the line of sight from AP-to-AP or AP-to-user). APs are placed equally spaced in two rows and users are scattered uniformly and at random in the whole floor (see Figure 5b). The distributed MU-MIMO system clearly outperforms the non-coordinated solution in terms of average per user throughput as can be seen in Figure 11a. It is interesting to notice that in contrast to the previous case, increasing the number of APs even up to 40 gives some gains for the non-coordinated systems under the CSMA scheduling scenario (see Figure 11b). From Figure 11c it is apparent that when the

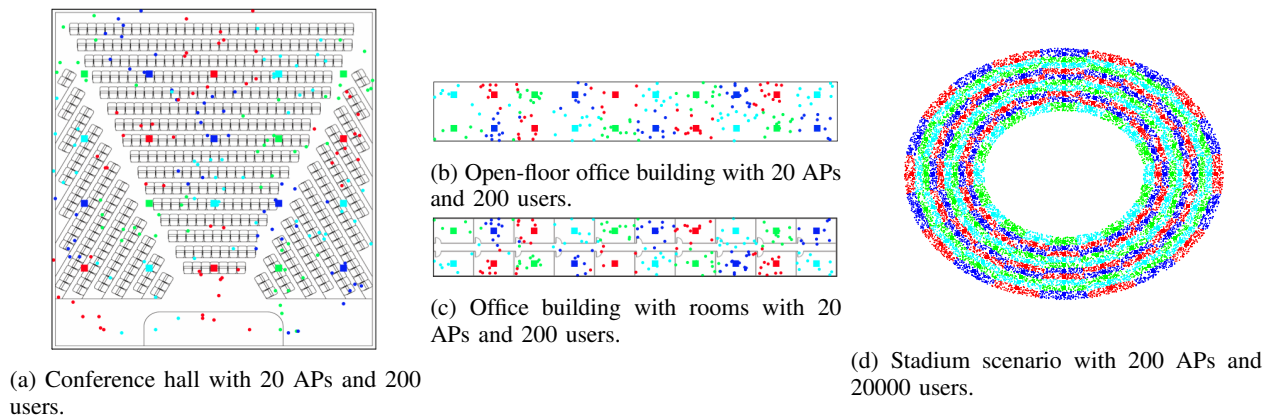


Fig. 5: AP placement, channel allocation and user-to-AP assignment for the scenarios examined.

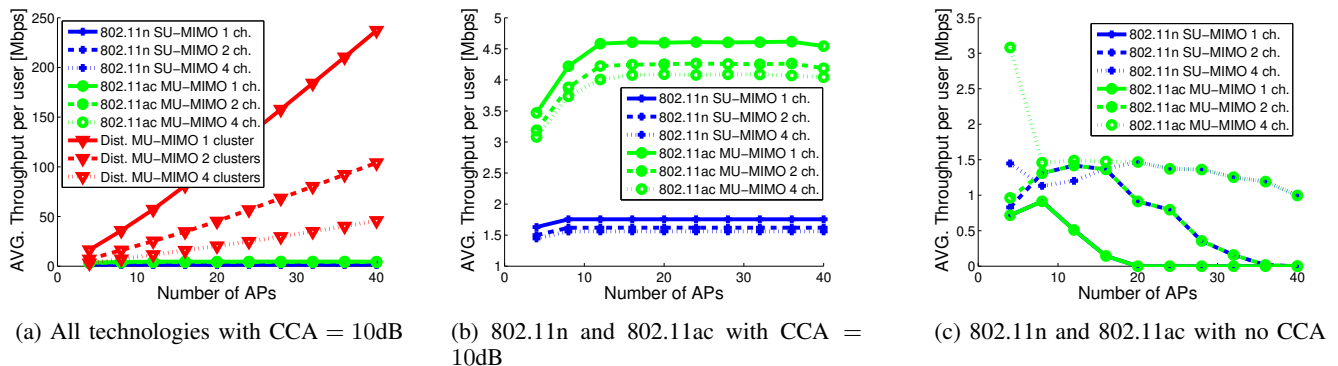


Fig. 6: Average throughput per user in a conference hall with 200 users varying CCA thresholds and 90dB transmit power.

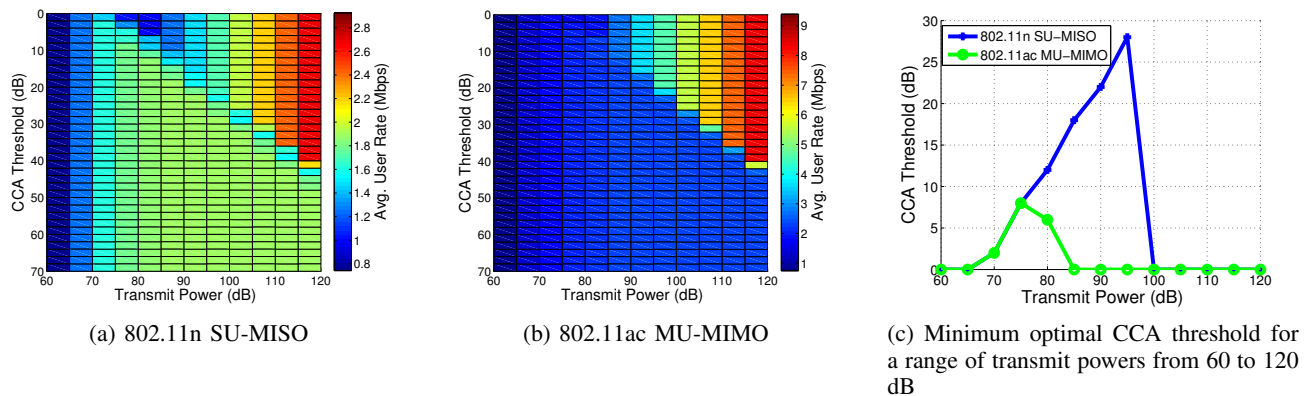


Fig. 7: CCA threshold and transmit power optimization for 802.11n SU-MISO and 802.11ac MU-MIMO.

CCA threshold is removed all together, the regime becomes interference limited as before. This can be seen by the rate degradation of the single channel system when adding more than 20 APs in the topology.

At this point we must emphasize the impact of using quantized rates in comparison to the information theoretic Gaussian rates. Although the latter offer a starting point to solve complex optimization problems and attain intuition for physical layer effects, they might lead to misleading intuition if not combined with an actual quantized mapping. Specifically, the scenarios with no CCA threshold (see Figures 11c for

the open-floor office building and 6c for the conference hall scenario) would look significantly different in their respective Gaussian versions. The rates would still saturate, but even at very low SINR, when the MCS mapping would give rates equal to zero, the Gaussian rate would assign some positive rate to every user. Further, increasing the number of APs increases the number of users served simultaneously (up to some limit), so the use of Gaussian rates leads to computing a higher average rate per user than what a quantized rate scheme would give.

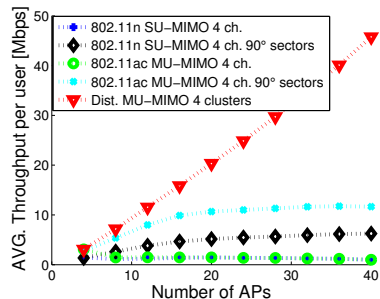


Fig. 8: Average throughput per user in a conference hall with and without sectorization with transmit power of 90dB and no CCA.

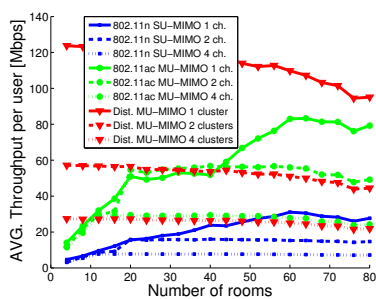


Fig. 9: Average throughput per user for an office building with rooms with transmit power of 90dB and CCA = 10dB.

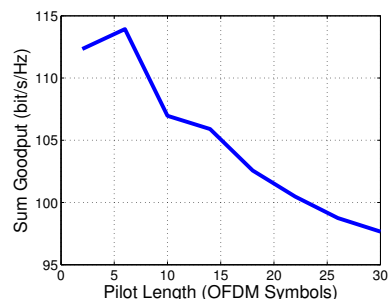
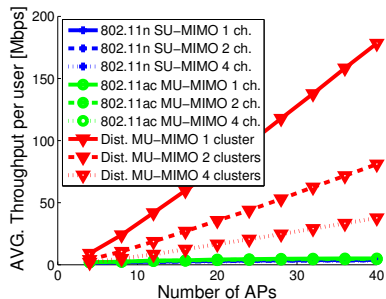
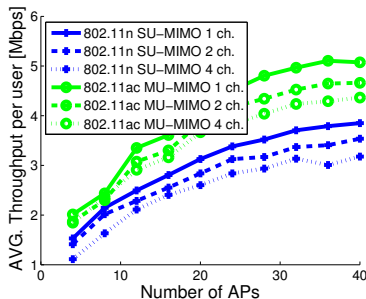


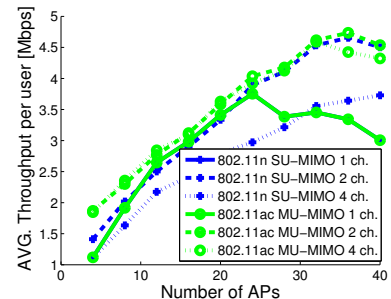
Fig. 10: Distributed MIMO overhead tradeoff due to synchronization and calibration requirements.



(a) All technologies with CCA = 10dB

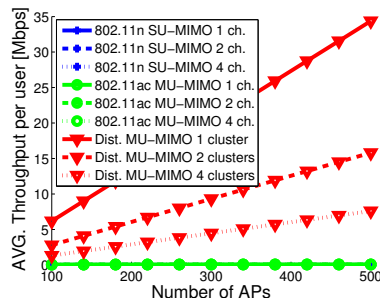


(b) 802.11n SU-MISO and 802.11ac MU-MIMO with CCA = 10dB

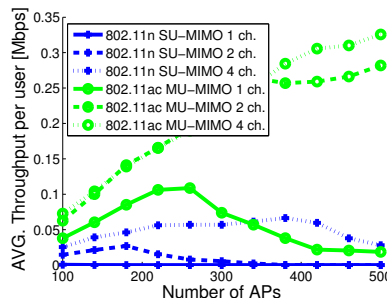


(c) 802.11n SU-MISO and 802.11ac MU-MIMO with no CCA

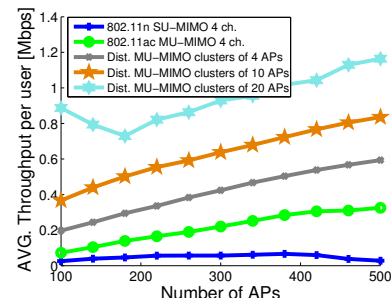
Fig. 11: Average throughput per user for an open-floor office plan with transmit power of 90dB.



(a) All technologies with CCA = 2dB.



(b) 802.11n SU-MISO and 802.11ac MU-MIMO with no CCA.



(c) Average throughput per user for a stadium with small clusters consisting of neighboring APs only.

Fig. 12: Average throughput per user for a stadium with 20000 users and transmit power of 90dB.

#### D. Office building floor with rooms

A typical office building floor with two rows of rooms and a corridor in between them (see Figure 5c) is analyzed with our model. The length of the floor is 160m, the width of each room is 10m, and the corridor width is 3m. For this series of experiments we fix the number of APs to 20 and users to 200 and investigate the behavior of the network as the number of rooms is varied. APs are placed in a canonical way to cover the whole area and users are scattered uniformly at random in the whole floor.

The increase of the number of rooms, while the floor dimensions and number of APs remains the same, essentially

adds additional barriers (walls) between APs. This, in return, effectively increases the pathloss between APs that share the same channel and thus significantly lowers the interference. On the other hand, the users fall out of line-of-sight with more APs, and in fact their pathlosses to many of the APs substantially increase due to the walls in between them. Thus, the multiplexing gains of distributed MU-MIMO disappear shortly after the number of rooms increases.

In Figure 9 we can see that as the APs become better separated by adding walls between them, the gains of distributed MU-MIMO are negligible and eventually trail behind the localized MU-MIMO scheme. This is expected since in

this scenario, only the gain with the AP assigned to each user is significant and thus, trying to beam form to users from distant APs, that are not in their transmit range, actually hurts the system instead of providing multiplexing gains.

### E. Stadium

Having the analytic model makes it easy and fast to compute the expected average user throughput in even larger scenarios as would be in the case of a football stadium (with a radius of 100m) during a big game (see Figure 5d for topology and channel assignment). We can imagine that at moments of high interest, for instance during a questionable refereeing decision or a touchdown, a large percentage of the in stadium fans might want to see a replay or a different camera feed online. In Figure 12a we can see the average throughput per user for a stadium of dimensions  $200\text{m} \times 200\text{m}$ , with 20000 users trying to access the internet and a range of APs. It is obvious in this case that only distributed MU-MIMO has the potential to provide an acceptable user service under such a challenging yet typical scenario. Moreover, if the CCA threshold is completely removed we again end up in an interference limited scenario where non-coordinated technologies suffer from rate saturation/degradation as the number of APs increases (see Figure 12b).

In such a large deployment, managing to coordinate hundreds of APs at the level of accuracy the distributed MU-MIMO architecture requires might be very challenging if not impossible in practice. Thus, a different approach consists of clustering only a small number of closely located APs in a distributed MU-MIMO cluster, and operating a large number of such clusters independently to cover the whole area. This has the effect of having clusters operating in the same frequency and not cooperating, thus creating interference to each other. Such deployments can also be efficiently analyzed using our model and the results can be seen in Figure 12c. We see that the performance of distributed MU-MIMO when APs are grouped in small clusters consisting of neighboring APs is significantly lower than that of a system coordinating all hundreds of APs together (compare Figures 12a and 12c). That said, it is still a lot better than uncoordinated MU-MIMO.

### F. Signaling overhead

**CSIT overhead:** It is worth noting that all the PHY schemes considered require the knowledge of channel state information at the transmitter side (CSIT) [30]. The overhead of the collection of CSIT exists and is similar in all aforementioned systems, but differs per topology and thus can only be taken into account in a per-scenario basis, it is thus not included in the analytic model. It is however straightforward to compute and discount for such an overhead based on the 802.11n/ac standards [37] and on some recent work of ours [31].

**Distributed MU-MIMO overhead:** Distributed MU-MIMO requires additional overhead to coordinate the APs in the cluster and allow them to operate as a single, virtual AP. In particular, timing and frequency synchronization (necessary for coherent distributed ZFBF) and uplink-downlink reciprocity (necessary to learn the downlink channel matrix

from the users uplink data packets) must be implemented through an efficient and scalable synchronization and calibration protocol. These problems have been recently addressed in depth in our work [31], as well as in a number of publications reporting software-defined radio prototype implementations of distributed MU-MIMO by us [3] and others [4], [42].

Practical synchronization between the APs is imperfect and residual carrier frequency offsets (CFOs) lead to a rate degradation that gets progressively worse over the course of transmission. Developing an analytical characterization of the tradeoff between the achievable rates and the synchronization overhead is difficult, since it is highly dependent upon the selection of “anchor” or leader nodes, and it involves non-convex optimization [31]. As such, this problem can be solved on a per-topology basis using simulations. Those that have been developed as part of our prior work [31].

Figure 10 illustrates the tradeoff between achievable rates and pilot overhead. This simulation is for the  $N_a = 20$  APs and  $K = 200$  users conference hall scenario (see Section VI-B), where clusters of  $B = 5$  APs form distributed MU-MIMO systems (see Section IV-E for details of clustering). We see that the optimal length of the synchronization sequence is 6 OFDM symbols, after which the longer sequences give diminishing returns in terms of synchronization quality, while consuming more overhead in the synchronization protocol and therefore reducing the system goodput. Thus each cluster needs 30 OFDM symbols of overhead for synchronization in the worst case, because the synchronization pilot signals need to be orthogonal in time.

In addition to synchronization overhead, distributed MIMO utilizes calibration between the APs in order to achieve uplink-downlink reciprocity [31], [45]. For a distributed MU-MIMO system, due to the residual CFOs, calibration pilot sequences must also be repeated at every downlink data slot [31]. In the previous example, we have determined that the optimal calibration sequence length is 4 OFDM symbols, for a total of 20 OFDM symbols per cluster. In general, for a given network configuration and distributed MU-MIMO clustering, it is possible to optimize “off-line” the overhead incurred by synchronization and calibration, and apply this overhead as a discount factor to calculate the goodput of the system.

## VII. CONCLUSIONS

In this paper we have introduced an accurate and practical analytical model for next generation wireless networks. We have applied the model in a variety of real-world scenarios and investigated the effect of all important system/design parameters to performance. An important result from this study is the significant performance gains that distributed MU-MIMO has over non coordinated approaches like concentrated MU-MIMO. That said, distributed MU-MIMO requires not only CSIT, but also tight synchronization and thus it incurs additional overhead. Also, in the presence of walls and other barriers which reduce inter-cell interference its gains are small, and, when considering a cap on the total number of APs that can be efficiently coordinated in practice, again its gains reduce. Other interesting outcomes of this work are the sizable

gains from sectorization, though to achieve those gains in practice, expensive front ends would have to be used (such front ends are typical in the context of cellular base stations but make less sense in the context of WiFi APs), as well as the speed by which non coordinated approaches become interference-limited resulting in no additional gains as more APs are added on the network. As a final point, it is evident from the depth and breath of the analysis of various practical scenarios in this work that our analytical model can be used to guide the deployment of future wireless networks and to optimize their performance.

## REFERENCES

- [1] Cisco, "Cisco Wireless LAN Controller Configuration Guide," Cisco Systems, Inc., Tech. Rep., 2013.
- [2] Aruba, "ArubaOS 6.2, User Guide," Aruba Networks, Inc., Tech. Rep., 2013.
- [3] H. V. Balan, R. Rogalin, A. Michaloliakos, K. Psounis, and G. Caire, "AirSync: Enabling Distributed Multiuser MIMO With Full Spatial Multiplexing," *IEEE/ACM Trans. Netw.*, vol. PP, no. 99, pp. 1–1, 2013.
- [4] H. S. Rahul, S. Kumar, and D. Katabi, "JMB: Scaling wireless capacity with user demands," *ACM SIGCOMM*, Aug. 2012.
- [5] H. Huh, A. Tulino, and G. Caire, "Network mimo with linear zero-forcing beamforming: Large system analysis, impact of channel estimation, and reduced-complexity scheduling," *IEEE Trans. Inf. Theory*, vol. 58, no. 5, pp. 2911–2934, 2012.
- [6] H. Huh, G. Caire, H. Papadopoulos, and S. Ramprasad, "Achieving massive MIMO spectral efficiency with a not-so-large number of antennas," *IEEE Trans. Wireless Commun.*, vol. 11, no. 9, pp. 3226–3239, 2012.
- [7] S. Ramprasad and G. Caire, "Cellular vs. network MIMO: A comparison including the channel state information overhead," in *IEEE PIMRC*, 2009.
- [8] S. Lakshminaryana, J. Hoydis, M. Debbah, and M. Assaad, "Asymptotic analysis of distributed multi-cell beamforming," in *IEEE PIMRC*, 2010.
- [9] F. Rusek, D. Persson, B. K. Lau, E. Larsson, T. Marzetta, O. Edfors, and F. Tufvesson, "Scaling up MIMO: Opportunities and challenges with very large arrays," *IEEE Signal Process. Mag.*, vol. 30, no. 1, pp. 40–60, 2013.
- [10] J. Hoydis, S. ten Brink, and M. Debbah, "Massive MIMO in the UL/DL of cellular networks: How many antennas do we need?" *IEEE J. Sel. Areas Commun.*, vol. 31, no. 2, pp. 160–171, 2013.
- [11] D. Gesbert, S. Hanly, H. Huang, S. Shamai Shitz, O. Simeone, and W. Yu, "Multi-Cell MIMO cooperative networks: A new look at interference," *IEEE J. Sel. Areas Commun.*, vol. 28, no. 9, pp. 1380–1408, 2010.
- [12] R. Zakhour and D. Gesbert, "Optimized data sharing in multicell MIMO with finite backhaul capacity," *IEEE Trans. Signal Process.*, vol. 59, no. 12, pp. 6102–6111, 2011.
- [13] P. de Kerret, R. Gangula, and D. Gesbert, "A practical precoding scheme for multicell MIMO channels with partial user's data sharing," in *IEEE WCNCW*, 2012.
- [14] J. Andrews, R. Ganti, M. Haenggi, N. Jindal, and S. Weber, "A primer on spatial modeling and analysis in wireless networks," *IEEE Commun. Mag.*, vol. 48, no. 11, pp. 156–163, 2010.
- [15] J. G. Andrews, S. Singh, Q. Ye, X. Lin, and H. S. Dhillon, "An overview of load balancing in HetNets: Old myths and open problems," *CoRR*, vol. abs/1307.7779, 2013.
- [16] H. S. Dhillon and J. G. Andrews, "Downlink rate distribution in heterogeneous cellular networks under generalized cell selection," *CoRR*, vol. abs/1306.6122, 2013.
- [17] H. Dhillon, R. Ganti, F. Baccelli, and J. Andrews, "Modeling and analysis of k-tier downlink heterogeneous cellular networks," *IEEE J. Sel. Areas Commun.*, vol. 30, no. 3, pp. 550–560, 2012.
- [18] G. Bianchi, L. Fratta, and M. Oliveri, "Performance evaluation and enhancement of the CSMA/CA MAC protocol for 802.11 wireless LANs," in *IEEE PIMRC*, 1996.
- [19] G. Bianchi, "Performance analysis of the ieee 802.11 distributed coordination function," *IEEE J. Sel. Areas Commun.*, vol. 18, no. 3, pp. 535–547, 2000.
- [20] E. Zouva and T. Antonakopoulos, "CSMA/CA performance under high traffic conditions: throughput and delay analysis," *Comput. Commun.*, vol. 25, no. 3, pp. 313 – 321, 2002.
- [21] R. Boorstyn, A. Kershenbaum, B. Maglaris, and V. Sahin, "Throughput analysis in multihop csma packet radio networks," *IEEE Trans. Commun.*, vol. 35, no. 3, pp. 267–274, Mar 1987.
- [22] S.-C. Liew, C. H. Kai, H. C. Leung, and P. Wong, "Back-of-the-envelope computation of throughput distributions in CSMA wireless networks," *IEEE Trans. Mobile Comput.*, vol. 9, no. 9, pp. 1319–1331, 2010.
- [23] L. Jiang and J. Walrand, "A distributed CSMA algorithm for throughput and utility maximization in wireless networks," *IEEE/ACM Trans. Netw.*, vol. 18, no. 3, pp. 960–972, 2010.
- [24] X. Wang and K. Kar, "Throughput modelling and fairness issues in CSMA/CA based ad-hoc networks," in *IEEE INFOCOM*, 2005.
- [25] A. Jindal and K. Psounis, "On the efficiency of csma-ca scheduling in wireless multihop networks," *IEEE/ACM Trans. Netw.*, vol. 21, no. 5, pp. 1392–1406, 2013.
- [26] —, "The achievable rate region of 802.11-scheduled multihop networks," *Networking, IEEE/ACM Transactions on*, vol. 17, no. 4, pp. 1118–1131, 2009.
- [27] D. H. Kang, K. W. Sung, and J. Zander, "Cost efficient high capacity indoor wireless access: Denser wi-fi or coordinated pico-cellular?" *CoRR*, vol. abs/1211.4392, 2012.
- [28] Y. Liang, A. Goldsmith, G. Foschini, R. Valenzuela, and D. Chizhik, "Evolution of base stations in cellular networks: Denser deployment versus coordination," in *IEEE ICC*, 2008.
- [29] Airmagnet, "Best practices for wireless site design," AirMagnet, Inc., Tech. Rep., 2007.
- [30] A. Molisch, *Wireless communications*. Wiley-IEEE, 2005.
- [31] R. Rogalin, O. Bursalioglu, H. Papadopoulos, G. Caire, A. Molisch, A. Michaloliakos, V. Balan, and K. Psounis, "Scalable synchronization and reciprocity calibration for distributed multiuser MIMO," *CoRR*, vol. abs/1310.7001, 2013.
- [32] P. Kyösti and et. al, "WINNER II channel models," Information Society Technologies, Tech. Rep., 2007.
- [33] G. Foschini and M. Gans, "On limits of wireless communications in a fading environment when using multiple antennas," *Wireless Pers. Commun.*, vol. 6, pp. 311–335, 1998.
- [34] E. Telatar, "Capacity of multi-antenna gaussian channels," *Eur. T. Telecommun.*, vol. 10, no. 6, pp. 585–595, 1999.
- [35] G. Caire and S. Shamai, "On the achievable throughput of a multiantenna gaussian broadcast channel," *IEEE Trans. Inf. Theory*, vol. 49, no. 7, pp. 1691 – 1706, Jul. 2003.
- [36] G. Caire, N. Jindal, M. Kobayashi, and N. Ravindran, "Multiuser MIMO Achievable Rates With Downlink Training and Channel State Feedback," *IEEE Trans. Inf. Theory*, vol. 56, no. 6, pp. 2845–2866, June 2010.
- [37] IEEE Computer Society, "IEEE Standard for IT - Telecommunications and Information Exchange Between Systems - LAN/MAN - Specific Requirements - Part 11: Wireless LAN MAC and PHY Layer Specifications - Amd 4: Enhancements for Very High Throughput for operation in bands below 6GHz," *IEEE Std 802.11ac-2013*.
- [38] Y. Bejerano, S.-J. Han, and L. Li, "Fairness and load balancing in wireless lans using association control," *IEEE/ACM Trans. Netw.*, vol. 15, no. 3, pp. 560–573, Jun. 2007.
- [39] R. Murty, J. Padhye, R. Chandra, A. Wolman, and B. Zill, "Designing high performance enterprise wi-fi networks," in *USENIX NSDI*, Berkeley, CA, 2008.
- [40] The Network Simulator NS-2. [Online]. Available: <http://www.isi.edu/nsnam/ns/>
- [41] H. Huang, M. Trivellato, A. Hottinen, M. Shafi, P. Smith, and R. Valenzuela, "Increasing downlink cellular throughput with limited network MIMO coordination," *IEEE Trans. Wireless Commun.*, vol. 8, no. 6, pp. 2983–2989, 2009.
- [42] X. Zhang, K. Sundaresan, M. A. A. Khojastepour, S. Rangarajan, and K. G. Shin, "NEMOX: Scalable Network MIMO for Wireless Networks," in *ACM MobiCom*, New York, NY, 2013.
- [43] H. Huh, H. Papadopoulos, and G. Caire, "Multiuser miso transmitter optimization for intercell interference mitigation," *IEEE Trans. Signal Process.*, vol. 58, no. 8, pp. 4272–4285, 2010.
- [44] K. Gilhousen, I. Jacobs, R. Padovani, A. Viterbi, J. Weaver, L.A., and I. Wheatley, C.E., "On the capacity of a cellular cdma system," *IEEE Trans. Veh. Technol.*, vol. 40, no. 2, pp. 303–312, May 1991.
- [45] C. Shepard, H. Yu, N. Anand, L. Li, T. Marzetta, R. Yang, and L. Zhong, "Argos: Practical many-antenna base stations," *ACM SIGCOMM*, Aug. 2012.